Review

Paweł Moskal* and Ewa Ł. Stępień

Positronium as a biomarker of hypoxia

Abstract: In this review article, we present arguments demonstrating that the advent of high sensitivity total-body PET systems and the invention of the method of *positronium imaging*, open realistic perspectives for the application of positronium as a biomarker for *in-vivo* assessment of the degree of hypoxia. Hypoxia is a state or condition, in which the availability of oxygen is not sufficient to support physiological processes in tissue and organs. Positronium is a metastable atom formed from electron and positron which is copiously produced in the intramolecular spaces in the living organisms undergoing positron emission tomography (PET). Properties of positronium, such as e.g., lifetime, depend on the size of intramolecular spaces and the concentration in them of oxygen molecules. Therefore, information on the partial pressure of oxygen (pO_2) in the tissue may be derived from the positronium lifetime measurement. The partial pressure of oxygen differs between healthy and cancer tissues in the range from 10 to 50 mmHg. Such differences of pO_2 result in the change of ortho-positronium lifetime e.g., in water by about 2–7 ps. Thus, the application of positronium as a biomarker of hypoxia requires the determination of the mean positronium lifetime with the resolution in the order of 2 ps. We argue that such resolution is in principle achievable for organ-wise positronium imaging with the total-body PET systems.

*Corresponding author: Paweł Moskal, M. Smoluchowski Institute of Physics, Faculty of Physics, Astronomy and Applied Computer Science, Jagiellonian University, Krakow, Poland; Total-Body Jagiellonian-PET Laboratory, Jagiellonian University, Kraków, Poland; and Theranostics Center, Jagiellonian University, Kraków, Poland, E-mail: p.moskal@uj.edu.pl. https://orcid.org/0000-0002-4229-3548
Ewa Ł. Stępień, M. Smoluchowski Institute of Physics, Faculty of Physics, Astronomy and Applied Computer Science, Jagiellonian University, Krakow, Poland; Total-Body Jagiellonian-PET Laboratory, Jagiellonian University, Kraków, Poland; and Theranostics Center, Jagiellonian University, Kraków, Poland, E-mail: e.stepien@uj.edu.pl. https://orcid.org/0000-0003-3589-1715

Introduction

A newly developed method of positronium imaging [1, 2], and the observation that positronium lifetime is changing inversely proportional with the concentration of oxygen in organic liquids [3, 4] opens new perspectives for *in-vivo* assessment of hypoxia.

Hypoxia is a state or condition, in which the availability of oxygen is not sufficient to support physiological processes in tissue and organs. It is a major feature of solid tumors, in which massive cell proliferation distances cells from the vasculature causing deficiency of blood carrying oxygen [5]. At a large distance from blood capillaries, the formed gradient of oxygen concentration is leading to reduced oxygen distribution, finally achieving severe hypoxia and causing cell death. Under intermediate conditions, such decreased oxygen availability diminishes the viability of cells. Oxygen diffusion within tissue is limited to only about 150 μm [5]. Therefore, in larger tumors, severe hypoxia is more likely to occur leading to form large necrotic zones of cells. Hypoxia is a good cancer prognostic indicator [6]. Hypoxia is also one of the fundamental factors related to the progression leading to the development of an aggressive phenotype, related to enhanced metastasis and treatment resistance [5–8]. In particular, the decreased oxygen concentrations in the cells increase the resistance to radiotherapy. This is because, under hypoxic conditions, the level of radiation-induced reactive oxygen species (ROS) may not be sufficient to cause significant damages to the cell structure (e.g., oxidative DNA damage) resulting in cell death [5]. Therefore, determination of the degree of hypoxia is an important factor to choose the appropriate cancer therapy [6], and it would be advantageous for patients to develop methods giving non-invasive *in-vivo* measurements of oxygen concentrations.

In Figure 1, a comparison of the partial pressure of oxygen molecules between healthy and neoplastic tissues is shown for brain, liver, prostate, kidney, head and neck, skin melanoma, cervical, lung, sarcoma, pancreas, and
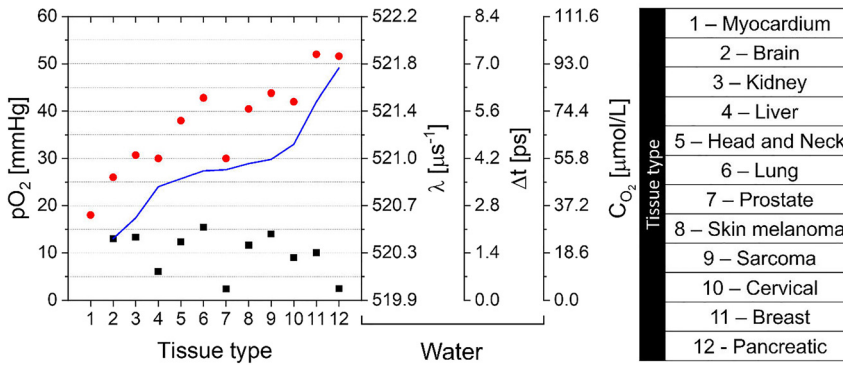
Figure 1: The partial pressure of oxygen molecules (pO_2) in healthy (red circles) and cancer (black squares) tissues. Numbers indicating tissue type are explained in the legend shown in the right panel. The blue curve presents the difference in partial pressure of oxygen between healthy and neoplastic tissues. The right axes of the figure present o-Ps annihilation rate (λ), changes of o-Ps mean lifetime (Δt) with respect to $pO_2 = 0$, and concentration of oxygen in water (C_{O_2}). The values λ and Δt shown on the right axes are calculated by formula 2 [3] assuming partial pressure of oxygen (pO_2) indicated on the left axis. The shown data do not reflect the real patients' variability and refers only to medians compiled from Refs. [7–13]. For the myocardium, only data for healthy tissue are known. Tissue types are ordered according to the increasing difference in oxygen partial pressure between healthy and cancerous tissues.

breast. For all these tissue types the partial pressure of oxygen (pO_2) in cancer tissues is several times lower than in corresponding healthy tissue. For healthy tissues, pO_2 is above 25 mmHg (reaching over 50 mmHg for pancreas and breast), while for cancer tissues pO_2 is below 15 mmHg (falling below 5 mmHg for pancreas and prostate). Thus, the observed differences in the partial pressure of oxygen in the healthy and neoplastic tissues are greater than 10 mmHg for all above-mentioned types of tissues and reach even 50 mmHg for the case of the pancreas.

At present, the tumor tissue oxygenation is measured invasively, e.g., by a polarographic oxygen electrode method (also called the Clark electrode), inserting a needle directly to the tumor [14]. The known *in-vivo* methods of assessing the degree of hypoxia, as the oxygenation-sensitive magnetic resonance [15], based on the estimation of deoxygenated hemoglobin in blood have limitations in the imaging of poorly vascularized tumors.

Currently, positron emission tomography (PET) is used only to some extent for non-invasive measurement of hypoxia by application of e.g., 64Cu-labeled ATSM, or ^{18}F-fluoromisonidazole (FMISO) radiotracer [2], especially for in head-and-neck cancers diagnosis [6, 13]. Recent introduction of positronium imaging [1, 2, 16–18] paved the way for *in-vivo* hypoxia imaging. The possibilities of positronium for assessing hypoxia were recently discussed by Shibuya [3] and Stepanov [4, 19]. In this article, we will argue that total-body PET [20–22] combined with positronium imaging method [1, 2, 22] opens a new prospect for *in-vivo* diagnosis of hypoxia *via* imaging of positronium properties in tumors during PET examination. In the next sections, we present (i) positronium characteristics relevant for its application as a hypoxia biomarker, (ii) a method of imaging of positronium properties in the living organisms and (iii) prospects for application of positronium as a biomarker of hypoxia.

Positronium formation and annihilation in the tissue

Positronium (Ps) is an atom composed of an electron and a positron. As an object made of matter and antimatter, it is not stable but annihilates into photons. The mean lifetime of positronium depends on its spin. In vacuum, it amounts to 142 ns for ortho-positronium (ground state with spin equal to 1) and 125 ps for para-positronium (the ground state with spin equal to 0) [23]. During the positron emission tomography, in about 40% of cases, positron emitted by the radionuclide attached to the radiopharmaceutical forms a positronium atom in a patient body [2, 24].

The process of positronium formation in the hemoglobin molecule is demonstrated in a pictorial way (Figure 2). Positron emitted by radionuclide (having energy at the order of 1 MeV) loses energy *via* ionization and excitation of atoms at the path of about 2 mm (e.g., in water the mean range of positrons emitted by ^{18}F is about 1.4 mm, and by [44]Sc it is about 2 mm [26]). At the end of positron thermalization, as the energy of the positron decreases, the distance between successive interaction places shortens to a few nm leading to the creation of the ionization blob
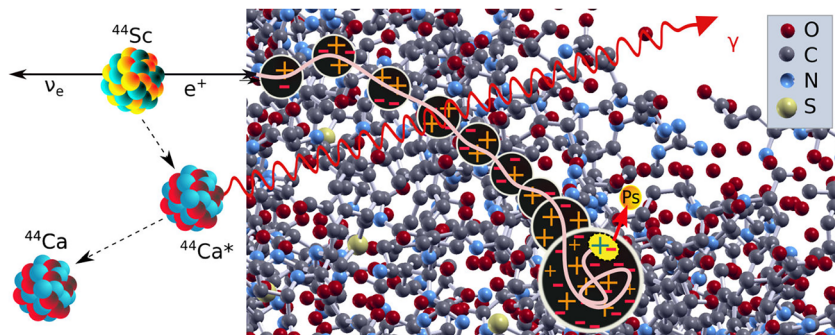
Figure 2: (Left panel) Schematic illustration of the decay of ^{44}Sc isotope which is one of the best-suited radionuclides for positronium imaging [22]. ^{44}Sc transforms into excited daughter nucleus ^{44}Ca* which deexcites through the emission of a prompt photon *via* the following process: ^{44}Sc → ^{44}Ca* $e^+ v → ^{44}$Ca $γ e^+ v$ [25]. The red arrow indicates prompt photon from the deexcitation of ^{44}Ca*. (Right panel) Illustration of positron (beige curve) thermalization at the end of its track in the hemoglobin molecule. Ionization sites composed of electrons (−) and ions (+) are shown. Quasi-free positronium (yellow dot including + −) formed in the blob localizes as positronium (yellow dot −Ps) in the intra-molecular void. Oxygen (O), carbon (C), nitrogen (N), and sulfur (S) atoms are indicated in colors as explained in the legend. Hydrogen atoms are not shown.

[27–29] which is composed of free electrons and cations. Thermalized positron having energy in the order of tens of eV may form in a blob a quasi-free positronium state (marked in Figure 2 in a yellow dot), which may diffuse into a nearby void as it is demonstrated in Figure 2 [19, 30].

Positronium may localize in the void both as ortho-positronium and as para-positronium. Due to the spin-statistics, the formation of ortho-positronium is three times more probable than the formation of para-positronium. The self-annihilation rate of para-positronium ($λ_{\text{p-Ps-self}}$ = 7,990.9 μs^{-1}) [31] is more than thousand times larger with respect to ortho-positronium ($λ_{\text{o-Ps-self}}$ = 7.0401 μs^{-1}) [32]. Therefore, the additional processes available in biological samples occurring with the rate of about 500 μs^{-1}, are affecting significantly only the mean ortho-positronium lifetime (which changes from 142 ns in vacuum to few ns in tissue) while the mean lifetime of para-positronium changes only by tens of ps. Therefore, it is the ortho-positronium state which may serve as a biomarker of tissue pathology.

Positronium trapped in the intra-molecular void, in addition to self-annihilation, may undergo disintegration *via* interaction with electrons from the surrounding molecular environment. The most significant additional processes are pick-off, conversion, and oxidation, illustrated pictorially in Figure 3. In the pick-off process [33] positron from positronium annihilates with electrons from the surrounding atom. The decay rate constant ($λ_{\text{pick-off}}$) describing the pick-off contribution of the positronium annihilation depends on the size of the free void. The relation between the positronium lifetime and the pore size D is presented in
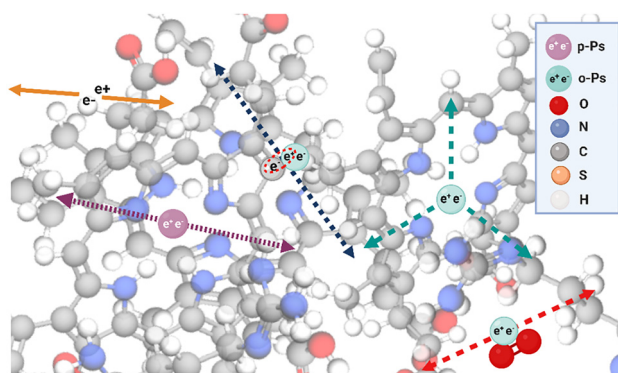

Figure 3: Basic (most probable) processes of positron and positronium annihilation in the intra-molecular voids of the hemoglobin molecule. Yellow solid arrows indicate photons from the direct positron–electron annihilation. Para-positronium (p-Ps) undergoes predominantly self-annihilation into two photons (violet dotted arrows). In the case of ortho-positronium, the most probable processes are pick-off annihilation to two photons (blue dashed arrows), o-Ps self-annihilation of to three photons (green dashed arrows), and conversion of o-Ps to p-Ps on O_2 molecule and subsequent annihilation into two photons (red dashed arrows). The size of atoms is shown to scale with the diameter of positronium twice as large as hydrogen.

Figure 4. It indicates that in biological samples, the free inter- and intra-molecular spaces are typically smaller than 1 nm. Positronium in the tissue, in addition to the pick-off process, may take part in chemical reactions with radiolytic products (e.g., H_3O^+, OH-radicals, hydrated electrons) and with other dissolved substances [4]. In particular, reactions of positronium with dissolved molecular oxygen O_2 may proceeded *via* conversion reaction (o-Ps + O_2 ↔ p-Ps + O_2) or
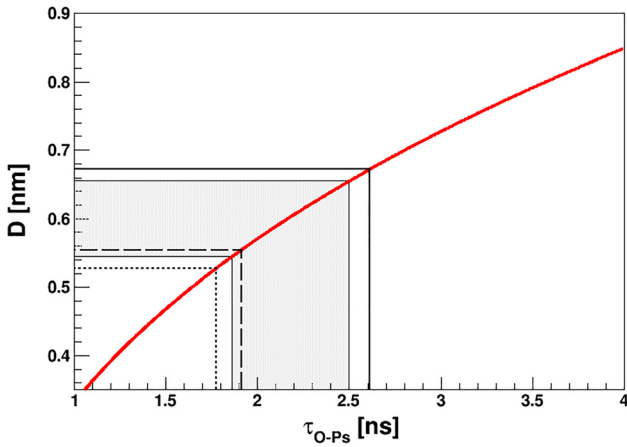
Figure 4: Diameter of voids D as a function of the ortho-positronium lifetime $\tau_{\text{o-Ps}}$ in biological samples calculated according to Tao–Eldrup model [34, 35]:

oxidation process ($Ps + O_2 \rightarrow e^+ + O_2^-$). These reactions constitute the basis for the application of positronium as a biomarker of hypoxia since they make the rate of positronium annihilation in the tissue dependent on the concentration of molecular oxygen. Recently Shibuya et al. [3] and Stepanov et al. [4, 19] have established that the positronium annihilation rate due to conversion ($\lambda_{\text{conversion}}$), oxidation ($\lambda_{\text{oxidation}}$), and other processes due to the presence of oxygen (λ_{O2other}) depends linearly on the concentration of dissolved O_2 (C_{O2}) for water [3, 4] and for organic liquids as cyclohexane, isooctane, and isopropanol [4, 19]:

$$\lambda_{O2} = \lambda_{\text{conversion}} + \lambda_{\text{oxidation}} + \lambda_{\text{O2other}} = k_{O2} \cdot C_{O2} \quad (1)$$

The coefficient k_{O2} established for water is equal to $0.0197 \pm 0.0006 \, \mu\text{mol}^{-1}\mu\text{s}^{-1}\text{L}$ (calculated as weighted mean of $k_{O2} = 0.0204 \pm 0.0008 \, \mu\text{mol}^{-1}\mu\text{s}^{-1}\text{L}$ [3] and $k_{O2} = 0.0186 \pm 0.0010 \, \mu\text{mol}^{-1}\mu\text{s}^{-1}\text{L}$ [4]) (It is worth noting that k_{O2} is much larger for other studied organic liquids [19]). Equivalently, Shibuya et al. [3] established practical formula for the estimation of partial pressure of oxygen in water based on the measured rate λ of o-Ps in water:

$$pO_2[\text{mmHg}] = k_{pO2} \cdot (\lambda(pO_2) - 519.9\,(16)\mu\text{s}^{-1}), \quad (2)$$

where ($\lambda(pO_2 = 0) = 519.9(16) \, \mu\text{s}^{-1}$), accounts for o-Ps self-annihilation and pick-off rate in water, and $k_{pO2} = 26{,}3\,(11)$ mmHg μs is equivalent to $k_{O2} = 0.0204 \pm 0.0008 \, \mu\text{mol}^{-1}\mu\text{s}^{-1}\text{L}$ [3]. Figure 1 indicates the relation between pO_2 and λ, Δt, C_{O2}. Δt denotes changes of o-Ps mean lifetime with respect to $pO_2 = 0$ which may be calculated as $\Delta t(pO_2) = 1/\lambda(pO_2 = 0) - 1/\lambda(pO_2)$, and $C_{O2} \, [\mu\text{mol/L}] = 1.89 \, pO_2 \, [\text{mmHg}]$ for water at 19° [3].

The total decay rate of positronium in tissue (λ_{tissue}), determining the mean lifetime τ_{tissue}, is due to the

positronium self-annihilation (λ_{self}), pick-off process ($\lambda_{\text{pick-off}}$), ortho-para conversion reactions ($\lambda_{\text{conversion}}$) and other chemical processes as e.g., oxidation ($\lambda_{\text{oxidation}}$):

$$\lambda_{\text{tissue}}(D, C_{O2}) = \frac{1}{\tau_{\text{tissue}}(D, C_{O2})}$$
$$= \lambda_{\text{Ps-self}} + \lambda_{\text{pick-off}}(D) + \lambda_{O2}(C_{O2})$$

The pick-off process reflects the distribution of the size of free voids in molecules (D) while conversion and oxidation processes depend on the oxygen concentration (C_{O2}). In water with saturated O_2 (1,400 μmol/L), when the conversion and oxidation is maximal, the relative strength of decay rates is as follows:

$$\lambda_{\text{p-Ps-self}}(7990.9\,\mu\text{s}^{-1}) \gg \lambda_{\text{pick-off}}(512.8\,\mu\text{s}^{-1}) \gg \lambda_{O2}(28\,\mu\text{s}^{-1})$$
$$> \lambda_{\text{o-Ps-self}}(7.0401\,\mu\text{s}^{-1})$$

$$\frac{1}{\tau_{\text{o-Ps}}} = 2\,\text{ns}^{-1}\left(1 - \frac{D}{(D+0.332)} + \sin\left(\frac{2\pi D}{(D+0.332)}\right)\middle/ 2\pi\right)$$

In pure water, the o-Ps lifetime decreases from 1.94 to 1.77 ns when the temperature increases from 0° to 40° [36]. Here, data are presented for water at 37° (dotted line) $\tau_{\text{o-Ps}} = 1.775$ ns, $D = 0.528$ nm [36]; myxoma (dashed line) and adipose tissue (solid line) at ambient temperature: $\tau_{\text{o-Ps}} = 1.91$ ns, $D = 0.554$ nm and $\tau_{\text{o-Ps}} = 2.61$ ns, $D = 0.672$ nm, respectively. Shadowed area represents data for biomembranes at 37° in aqueous solution, like DPPC:Cholesterol (60:40): $\tau_{\text{o-Ps}} = 1.86$ ns, $D = 0.545$ nm [37] and DPPC:Ceramides (85:15) $\tau_{\text{o-Ps}} = 2.5$ ns, $D = 0.655$ nm [38]. As we may see from the example of the hemoglobin molecule (Figures 2 and 3) being a part of the erythrocytes, the shape of voids is irregular and their size varies. The measured mean o-Ps lifetime is a measure of the mean lifetimes averaged over the full voids size distribution, thus D is only an effective parameter of pore size in water solution [36]. The relation between the positronium lifetime and the pore size D is very well described by the Tao–Eldrup model [34, 35] for D less than 2 nm [39]. Therefore, this model is very well suited for the description of biological samples where the free inter- and intra-molecular spaces are typically smaller than 1 nm.

Positronium imaging

Positronium imaging is a novel tomography method enabling *in-vivo* imaging of positronium properties such as mean lifetime, production probability, and 3-photon/2-photon rate ratio in living organisms [1, 2, 16, 17, 24]. The first *in-vitro* positronium 2-photon [2] and 3-photon [18] images have been

determined by means of the 192-strip J-PET prototype. J-PET is a first multi-photon PET system built from plastic scintillators [40–46]. The information comprised in positronium images concerns the size of intramolecular voids and concentration in them of bio-active molecules and it is qualitatively different from the anatomical and morphological images obtainable by computed tomography (CT) and magnetic resonance imaging (MRI).

The two or three photons from the positronium decay are used for the reconstruction of the annihilation density distribution, while the positronium lifetime may be determined when the administered radionuclide emits additional gamma quantum carrying information of the time of positronium formation. In Ref. [22] it was argued that ^{44}Sc is one of the most suitable isotopes for positronium imaging. ^{44}Sc isotope emits positron (e^+) and prompt gamma (γ) via following process: ^{44}Sc $\rightarrow$ ^{44}Ca$\star$ e^+ ν $\rightarrow$ ^{44}Ca γ e^+ ν [25]. ^{44}Sc may be attached e.g., to the prostate-specific membrane antigen (PSMA-617 ligand) characterized by high affinity to the PSMA receptors highly expressed in prostate epithelial cells [22, 47].

There are investigations demonstrating differences between normal and cancerous cells with changes of the positronium lifetime during dynamical processes undergoing in model and living biological systems [2, 48–55]. These results indicate that positronium imaging may be useful for the assessment of tissue alterations at the molecular level before they lead to functional and morphological changes [22]. Moreover, it was recently shown that positronium lifetime is changing inversely proportional with the concentration of oxygen in organic liquids [3, 4] indicating its potential for detecting and quantifying hypoxia.

Figure 5 presents exemplary events of electron-positron annihilations in the patient's body. The figure shows the photo of a recently commissioned modular J-PET tomograph built from plastic scintillators with superimposed red solid arrows indicating exemplary annihilation photons and dashed arrows indicating prompt gamma from the decay of ^{44}Sc isotope. The registration of prompt gamma enables to determine the time of the positron emission (which within picoseconds is equivalent to the time of the positronium formation). Coincident measurement of annihilation photons enables the reconstruction of the time and position of positronium decay separately for each voxel of the imaged object. As discussed in the
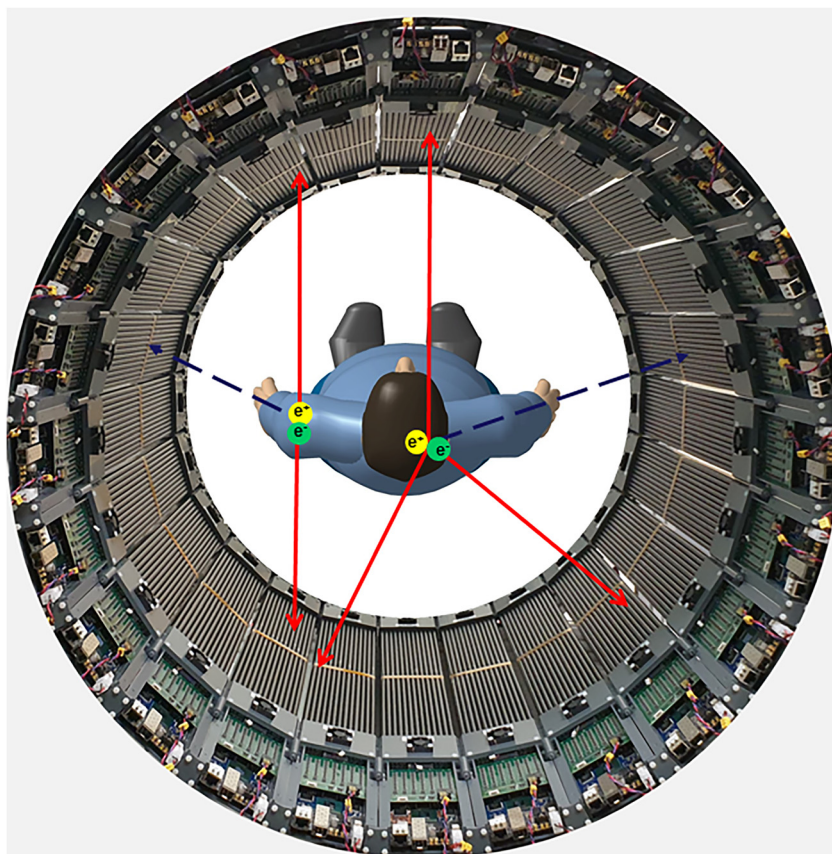

Figure 5: Photograph of the single layer (with 50 cm AFOV) modular J-PET prototype with superimposed representations of electron–positron annihilation in the patient's body for two and three-photon events (red solid arrows) and the associated prompt gamma rays (blue dashed arrows) emitted by the $\beta^+\gamma$ radionuclide such as e.g., ^{44}Sc. The single-layer J-PET prototype with AFOV = 50 cm weighs only about 60 kg. It consists of 24 modules each built from plastic scintillator strips (black) read out at both ends by SiPMs equipped with the dedicated front-end and digitizing electronics visible in the foreground [56, 57]. The trigger-less data acquisition system of the modular J-PET tomograph [57] enables detection of all events including multi-photon annihilations and prompt gammas, not restricted to the standard double annihilation photons coincidences as it is in the current PET scanners.

previous section, the degree of hypoxia may be estimated based on the measurement of the mean lifetime of o-Ps atoms. As shown in Figure 3, in the tissue o-Ps undergo self-annihilation into three photons and annihilations into two photons via pick-off and conversion processes. Therefore, the image of the mean lifetime of positronium may be reconstructed for the 3-photon as well as for 2-photon annihilations. Recently the first 3-photon and 2-photon positronium images were demonstrated by means of the J-PET scanner [2, 18].

Prospects for application of positronium as a biomarker of hypoxia

In previous sections, we argued that the mean lifetime of ortho-positronium is a promising biomarker of hypoxia and that positronium imaging enables imaging of ortho-positronium lifetime in the living organism. During PET diagnosis of a living organism, the annihilation of positrons proceeds via the formation of ortho-positronium in about 30% of cases [7, 24]. In a vacuum, o-Ps decays predominantly into three photons. On the contrary, due to the pick-off and conversion processes in the tissue, most of the decays of o-Ps are into two-photons, and in the tissue, 3-photon decays constitute only about 0.5% of all decays including 0.25% originating from 3-photon decays of o-Ps. The ratio of 3-photon to 2-photon decays was considered as an indicator of hypoxia in 2005 by Kacperski and Spyrou [58] who proposed a method to reconstruct the position of e^+e^- annihilation into three photons based on the measurement of photons' energies and positions of interactions with high-resolution semiconductor detectors (such as e.g., CdZnTe). Yet, it was concluded that due to the low fraction of 3-photon events this method cannot provide the sensitivity needed to detect changes in the tissue of the dissolved oxygen concentrations [59]. Moreover, the construction of PET scanners from the semiconductor detectors would be even more expensive than crystal-based PET systems.

Recently demonstrated positronium imaging method opens the new promising prospect for application of positronium as a biomarker of hypoxia [2]. This is because this method may be used by cost-effective plastic-based PET systems and it enables reconstruction of images of a mean o-Ps lifetime based on 2-photon annihilations. Figure 6 compares imaging sensitivity for standard 2-photon PET and 2-photon positronium imaging as a function of the axial field-of-view of the scanner [22]. It
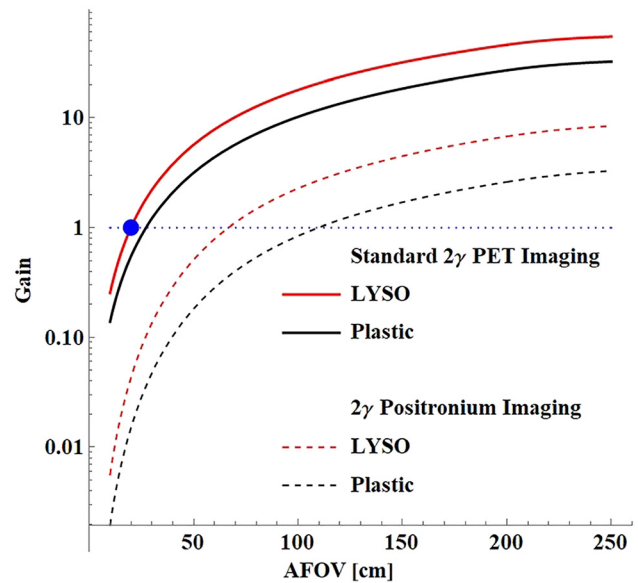

Figure 6: Sensitivity gain in PET and positronium imaging as a function of the axial field-of-view (AFOV) of the scanner [22]. Results for crystal (LYSO) PET and plastic PET are shown with respect to the 20 cm AFOV LYSO PET (indicated with horizontal blue dotted line).

indicates that, when using a cost-effective total-body PET from plastic scintillators with a length of 2 m, the sensitivity for 2-photon positronium imaging will be about two times higher than the sensitivity for the standard 2-photon PET imaging with the 20 cm long LYSO crystal PET. This conclusion is valid for whole-body imaging. Thus, Figure 6 indicates that as regards whole-body imaging, the total-body PET systems provide sufficient sensitivity for 2-photon positronium imaging with the statistics of events comparable with the present 2-photon standard PET with a 20 cm axial field of view.

The degree of hypoxia may be assessed provided that the time resolution for the mean o-Ps lifetime will be high enough to distinguish between the hypoxic and normoxic conditions.

Figure 1 shows that the partial pressure of oxygen differs between healthy and cancer tissues in the range from 10 mmHg (for the brain) to 50 mmHg (for the pancreas). Using relationships between the partial oxygen pressure pO_2 and the o-Ps decay rate constant (recently established by Shibuya et al. [3] and Stepanov et al. [4, 19]) one can estimate that such differences in partial pressure of oxygen are corresponding to the change of ortho-positronium lifetime e.g., in water by about 2–7 ps (see Figure 1 and Eq. (2)). Thus, the application of ortho-positronium as a biomarker of hypoxia requires the determination of the mean positronium lifetime with the resolution in the order of 2 ps. This is rather a pessimistic estimation assuming that tissues are from the

water. For a more realistic assessment, *in-vivo* studies of positronium properties in living organisms are required.

It was shown in Ref. [17] that the resolution for the determination of the mean o-Ps lifetime depends predominantly on the value of this mean o-Ps lifetime in the tissue (τ_{oPs}). Therefore, it can be estimated as $\tau_{oPs}/sqrt(N)$, with N denoting the number of events in a given voxel of the positronium image. The mean lifetime in the tissue τ_{oPs} is in the order of 2 ns (see Figure 4) and for the total body PET systems about 10^4 events in positronium image per cm^3 voxel are expected [17]. Therefore, we expect a resolution of about 20 ps which (employing Eq. (2)) is equivalent to the sensitivity for the oxygen partial pressure estimation of about 140 mmHg. Therefore, in order to distinguish between hypoxic and normoxic conditions, a 100 fold higher number of registered events (10^6) would be required which would allow achieving a resolution of about 14 mmHg. Such statistics could be achievable for an organ-wise estimation of hypoxia with positronium as a biomarker. For example, for the pancreas with a volume of about 100 cm^3, 10^6 o-Ps events could be registered using total-body PET enabling estimation of the o-Ps lifetime in the pancreas with 2 ps resolution.

Conclusions

In this communication, we discuss prospects of the application of positronium as a biomarker of hypoxia. We presented arguments that the newly demonstrated 2-photon positronium imaging method [2, 18] applied in the total body PET systems [60] may enable organ-wise *in-vivo* assessment of the degree of hypoxia by imaging of the mean lifetime of ortho-positronium.

Author contributions: All authors have accepted responsibility for the entire content of this manuscript and approved its submission.
Competing interests: Authors state no conflict of interest.
Informed consent: Informed consent was obtained from all individuals included in this study.

Ethical approval: The local Institutional Review Board deemed the study exempt from review.

References

1. Moskal P. Positronium imaging. In: 2019 IEEE nuclear science symposium and medical imaging conference (NSS/MIC). IEEE Xplore, Manchester, UK; 2020.

2. Moskal P, Dulski K, Chug N, Curceanu C, Czerwiński E, Dadgar M, et al. Positronium imaging with the novel multiphoton PET scanner. Sci Adv 2021;7:eabh4394.

3. Shibuya K, Saito H, Nishikido F, Takahashi M, Yamaya T. Oxygen sensing ability of positronium atom for tumor hypoxia imaging. Commun Phys 2020;3:1–8.

4. Stepanov P, Selim F, Stepanov S, Bokov A, Ilyukhina O, Duplâtre G, et al. Interaction of positronium with dissolved oxygen in liquids. Phys Chem Chem Phys 2020;22:5123–31.

5. Brahimi-Horn CM, Chiche J, Pouysségur J. Hypoxia and cancer. J Mol Med 2007;85:1301–7.

6. Krolicki L, Kunikowska D. Theranostics – present and future. Bio Algorithm Med Syst 2021;17:213–20.

7. Vaupel P, Flood AB, Harold, Swartz HM. Oxygenation status of malignant tumors vs. normal tissues: critical evaluation and updated data source based on direct measurements with pO2. Appl Magn Reason 2021;52:1451–79.

8. McKeown SR. Defining normoxia, physoxia and hypoxia in tumours - implications for treatment response. Br J Radiol 2014; 87:20130676.

9. Swartz HM, Flood AB, Schaner PE, Halpern H, Williams BB, Pogue BW, et al. How best to interpret measures of levels of oxygen in tissues to make them effective clinical tools for care of patients with cancer and other oxygen-dependent pathologies. Phys Rep 2020;8:e14541.

10. Becker A, Hansgen G, Bloching M, Weigel C, Lautenschlager C, Dunst J. Oxygenation of squamous cell carcinoma of the head and neck: comparison of primary tumors, neck node metastases, and normal tissue. Int J Radiat Oncol Biol Phys 1998;42:35.

11. Nordsmark M, Bentzen SM, Overgaard J. Measurement of human tumour oxygenation status by a polarographic needle electrode. An analysis of inter- and intratumour heterogeneity. Acta Oncol 1994;33:383–9.

12. Lartigau E, Randrianarivelo H, Avril MF, Margulis A, Spatz A, Eschwege F, et al. Intratumoral oxygen tension in metastatic melanoma. Melanoma Res 1997;7:400–6.

13. Lawrentschuk N, Poon AM, Foo SS, Putra LG, Murone C, Davis ID, et al. Assessing regional hypoxia in human renal tumours using 18F-fluoromisonidazole positron emission tomography. BJU Int 2005;96:540–6.

14. Nakano T, Suzuki Y, Ohno T, Kato S, Suzuki M, Morita S, et al. Carbon beam therapy overcomes the radiation resistance of uterine cervical cancer originating from hypoxia. Clin Cancer Res 2006;12:2185–90.

15. Friedrich MG, Karamitsos TD. Oxygenation-sensitive cardiovascular magnetic resonance. J Cardiovasc Magn Reason 2013;15:43.

16. Moskal P, Kisielewska D, Curceanu C, Czerwiński E, Dulski K, Gajos A, et al. Feasibility study of the positronium imaging with the J-PET tomograph. Phys Med Biol 2019;64:055017.

17. Moskal P, Kisielewska D, Shopa RY, Bura Z, Chhokar J, Curceanu C, et al. Performance assessment of the 2γ positronium imaging with the total-body PET scanners. EJNMMI Phys 2020;7:1–16.

18. Moskal P, Gajos A, Mohammed M, Chhokar J, Chug N, Curceanu C, et al. Testing CPT symmetry in ortho-positronium decays with positronium annihilation tomography. Nat Commun 2021;12:5658.

19. Stepanov SV, Byakova VM, Stepanov PS. Positronium in biosystems and medicine: a new approach to tumor diagnostics based on correlation between oxygenation of tissues and lifetime of the positronium atom. Phys Wave Phenom 2021;29:174.

20. Badawi RD, Shi H, Hu P, Chen S, Xu T, Price PM, et al. First human imaging studies with the EXPLORER total-body PET scanner. J Nucl Med 2019;60:299.

21. Karp JS, Viswanath V, Geagan MJ, Muehllehner G, Pantel AR, Parma MJ, et al. PennPET explorer: design and preliminary performance of a whole-body imager. J Nucl Med 2020;61:136–43.

22. Moskal P, Stępień E. Prospects and clinical perspectives of total body PET imaging using plastic scintillators. Pet Clin 2020;15:439–52.

23. Bass SD. QED and fundamental symmetries in positronium decays. Acta Phys Pol B 2019;50:1319.

24. Moskal P, Jasińska B, Stępień EŁ, Bass SD. Positronium in medicine and biology. Nat Rev Phys 2019;1:527–9.

25. Matulewicz T. Radionuclide candidates for theranostics: an overview. Bio Algorithm Med Syst 2021;17. https://doi.org/10.1515/bams-2021-0142.

26. Thirolf PG, Lang C, Parodi K. Perspectives for highly-sensitive PET-based medical imaging using β+γ coincidences. Acta Phys Pol, A 2015;127:1441–4.

27. Byakov VM, Stepanov SV. Common features in the formation of Ps, Mu, radiolytic hydrogen and solvated electrons in aqueous solutions. J Radioanal Nucl Chem 1996;210:371–405.

28. Stepanov SV, Byakov VM. Electric field effect on positronium formation in liquids. J Chem Phys 2002;116:6178–95.

29. Goworek T. Positronium as a probe of small free volumes in crystals, polymers and porous media. Ann Univ Mariae Curie-Sklodowska 2014;69:1–110.

30. Stepanov SV, Zvezhinskiy DS, Byakov VM, Duplatre G, Stepanov PS. Positrons and positronium atoms in a condensed phase close to its melting point. Acta Phys Pol, A 2014;125:691–5.

31. Kataoka Y, Asai S, Kobayashi T. First test of O(α2) correction of the orthopositronium decay rate. Phys Lett B 2009;671:219–23.

32. Al-Ramadhan AH, Gidley DW. New precision measurement of the decay rate of singlet positronium. Phys Rev Lett 1994;72:1632–5.

33. Garwin RL. Thermalization of positrons in metals. Phys Rev 1953;91:1571.

34. Tao SJ. Positronium annihilation in molecular substances. J Chem Phys 1972;56:5499.

35. Eldrup MM, Lightbody D, Sherwood JN. The temperature dependence of positron lifetimes in solid pivalic acid. Chem Phys 1981;63:51–8.

36. Kotera K, Saito T, Yamanaka T. Measurement of positron lifetime to probe the mixed molecular states of liquid water. Phys Lett A 2005;345:184–90.

37. Sane P, Salonen E, Falck E, Repakova J, Tuomisto F, Holopainen JM, et al. Probing biomembranes with positrons. J Phys Chem B 2009;113:1810–2.

38. Axpe E, Garcia-Arribas AB, Mujika JI, Merida D, Alonso A, Lopez X, et al. Ceramide increases free volume voids in DPPC Membranes. RSC Adv 2015;5:44282–90.

39. Dull TL, Frieze WE, Gidley DW, Sun JN, Yee AF. Determination of pore size in mesoporous thin films from the annihilation lifetime of positronium. J Phys Chem B 2001;105:4657–62.

40. Moskal P, Salabura P, Silarski M, Smyrski M, Zdebik J, Zieliński M. Novel detector systems for the positron emission tomography. Bio Algorithm Med Syst 2011;7:73.

41. Moskal P, Kowalski P, Shopa RY, Raczyński L, Baran J, Chug N, et al. Simulating NEMA characteristics of the modular total-body J-PET scanner - an economic total-body PET from plastic scintillators. Phys Med Biol 2021;66:175015.

42. Moskal P, Bednarski T, Niedźwiecki SZ, Silarski M, Czerwiński E, Kozik T, et al. Synchronisation and calibration of the 24-modules J-PET prototype with 300 mm axial field of view. IEEE Trans Instrum Meas 2021;70:2000810.

43. Niedźwiecki S, Białas P, Curceanu C, Czerwiński E, Dulski K, Gajos A, et al. J-PET: a new technology for the whole-body PET imaging. Acta Phys Pol B 2017;48:1567–76.

44. Moskal P, Rundel O, Alfs D, Bednarski T, Białas P, Czerwiński E, et al. Time resolution of the plastic scintillator strips with matrix photomultiplier readout for J-PET tomograph. Phys Med Biol 2016;61:2025–47.

45. Moskal P, Zoń N, Bednarski T, Białas P, Czerwiński E, Gajos A, et al. A novel method for the line-of-response and time-of-flight reconstruction in TOF-PET detectors based on a library of synchronized model signals. Nucl Instrum Methods A 2015;775:54–62.

46. Moskal P, Niedźwiecki SZ, Bednarski T, Czerwiński E, Kapłon Ł, Kubicz E, et al. Test of a single module of the J-PET scanner based on plastic scintillators. Nucl Instrum Methods A 2014;764:317–21.

47. Rahbar K, Afshar-Oromieh A, Jadvar H, Ahmadzadehfar H. PSMA theranostics: current status and future directions. Mol Imag 2018;17:1536012118776068.

48. Kubicz E, Stępień E, Grudzień G, Dulski K, Leszczyński B, Moskal P. Positronium life-time as a new approach for cardiac masses imaging. Eur Heart J 2021;42(1 Suppl):ehab724.3279.

49. Moskal P, Kubicz E, Grudzień G, Czerwiński E, Dulski K, Leszczyński B, et al. Developing a novel positronium biomarker for cardiac myxoma imaging. bioRxiv 2021:455285. https://doi.org/10.1101/2021.08.05.455285.

50. Zgardzińska B, Chołubek G, Jarosz B, Wysogląd K, Gorgol M, Goździuk M, et al. Studies on healthy and neoplastic tissues using positron annihilation lifetime spectroscopy and focused histopathological imaging. Sci Rep 2020;10:11890.

51. Chen HM, van Horn JD, Jean YC. Applications of positron annihilation spectroscopy to life science. Defect Diffusion Forum 2012;331:275–93.

52. Jasińska B, Zgardzińska B, Chołubek G, Pietrow M, Gorgol M, Wiktor K, et al. Human tissue investigations using PALS technique - free radicals influence. Acta Phys Pol, A 2017;132:1556–8.

53. Kilburn D, Townrow S, Meunier V, Richardson R, Alam A, Ubbink J. Organization and mobility of water in amorphous and crystalline trehalose. Nat Mater 2006;5:632–5.

54. Jean YC, Li Y, Liu G, Chen H, Zhang J, Gadzia JE. Applications of slow positrons to cancer research: search for selectivity of positron annihilation to skin cancer. Appl Surf Sci 2006;252:3166–71.

55. Axpe E, Lopez-Euba T, Castellanos-Rubio A, Merida D, Garcia JA, Plaza-Izurieta L, et al. Detection of atomic scale changes in the free volume void size of three-dimensional colorectal cancer cell culture using positron annihilation lifetime spectroscopy. PLoS One 2014;9:e83838.

56. Pałka M, Strzempek P, Korcyl G, Bednarski T, Niedźwiecki SZ, Białas P, et al. Multichannel FPGA based MVT system for high precision time (20 ps RMS) and charge measurement. J Instrum 2017;12:P08001.

57. Korcyl G, Białas P, Curceanu C, Czerwiński E, Dulski K, Flak B, et al. Evaluation of single-chip, real-time tomographic data processing on FPGA SoC devices. IEEE Trans Med Imag 2018;37:2526–35.

58. Kacperski K, Spyrou NM. Performance of three-photon PET imaging: Monte Carlo simulations. Phys Med Biol 2005;50: 5679.

59. Mercurio K, Zerkel P, Laforest R, Sobotka LG, Charity RJ. The three-photon yield from e+ annihilation in various fluids. Phys Med Biol 2006;51:N323–9.

60. Vandenberghe S, Moskal P, Karp JS. State of the art in total body PET. EJNMMI Phys 2020;7:35.